UCRL-ID-141998

Simulations of SSPX Sustainment – Toward a Standard Model for Spheromaks

T. K. Fowler, D. D. Hua, and B. W. Stallard

January 12, 2001

U.S. Department of Energy

Lawrence
Livermore
National
Laboratory

DISCLAIMER

This work was performed under the auspices of the U. S. Department of Energy by the University of California, Lawrence Livermore National Laboratory under Contract No. W-7405-Eng-48.

SIMULATIONS OF SSPX SUSTAINMENT -- TOWARD A STANDARD MODEL FOR SPHEROMAKS*

T. K. Fowler, D. D. Hua and B. W. Stallard

January 12, 2001

Abstract

SPHERE simulations calibrated to CTX are shown to predict the correct temperature (0.12 KeV) for SSPX sustainment Shot 4624. Agreement with the temperature suggests that the Rechester-Rosenbluth thermal diffusivity included in the SPHERE heat transport equation is essentially correct. Substituting parallel heat loss as suggested by NIMROD calculations gives a temperature four times too low, while omitting Rechester-Rosenbluth transport but retaining ion classical transport gives a temperature that is 50% too high. Less certain is the magnetic buildup equation in SPHERE representing the spheromak load as a resistance adjusted to give the correct magnetic field -- as is essential to obtain the correct temperature by ohmic heating. While extrapolation for long pulses using the Shot 4624 resistance does give higher magnetic field and higher temperature, the actual resistance during sustainment is still highly uncertain. In Section 6, we present a new resistance model in rough agreement with Shot 4624, but much work remains to be done. Understanding the spheromak resistance during sustainment is the main theoretical challenge for the model.

* * * * *

1. Introduction

We have simulated SSPX Shot 4624 in which the electron temperature rises to 0.12 KeV during the Sustainment phase, using the SPHERE code [1]. Results are given in Figures 4 - 8, discussed in Section 3.

The gun circuit simulation for this shot is presented in Section 2. Extrapolations to long pulses are given in Section 4, followed in Section 5 by a critique of uncertainties and a review of SPHERE physics as a "standard model" for future work. Section 6 presents a new model for the spheromak resistance, and conclusions are given in Section 7.

2. Gun Circuit

The gun power is simulated by the simplified capacitor bank model in the SPHERE code with parameters chosen to reproduce approximately SPICE simulations of the gun circuit for Shot 4624, as follows:

---

*This work was performed under the auspices of the U.S. Department of Energy by the University of California, Lawrence Livermore National Laboratory under contract No. W-7405-Eng-48.

	Formation Bank	Sustainment Bank
C(farads)	0.01	0.096
L(μHenries)	1.1	2.225
R(mohms)	2.601	1.3
V(volts)	7000	1400

The delay to turn on of the Sustainment Bank is 300 microseconds.

In characterizing the plasma electrical load, we have in mind a flux core geometry consisting of an open-line flux core tied to the bias flux ψ, surrounded by a spheromak in the lowest Taylor state with eigenvalue $\lambda_o = 5/R$ with flux conserver radius R. As in SPICE simulations, we represent the flux core by a fixed inductance 0.6 μH, while the spheromak is represented by a variable resistance of the form:

$$R_S = \kappa(1 - I_o/I) \quad \text{(zero if negative)} \qquad (1)$$

giving as the power building up the spheromak magnetic field:

$$P = f I^2 R_S \qquad (2)$$

with gun efficiency

$$f = f_K (I_o/I) \quad . \qquad (3)$$

Here $I_o = \lambda_o\psi/\mu_o$ is the threshold current for instability and f_K represents the efficiency of injecting helicity from the gun into the main flux conserver volume. The factor I_o/I is the "fundamental efficiency" for converting gun power into helicity K and magnetic energy $E = (\lambda_o/2\mu_o)K$: $(dE/dt)/(I V_S) = I_o/I$ with $dK/dt = 2V_S\psi$ ($V_S = IR_S$). The spheromak resistance R_S is discussed in Section 6.

We take I_o = 180 KA and κ = 10 mΩ held constant throughout the Formation and Sustainment phases. These values were chosen to give the measured peak gun current (Figure 1) and measured gun energy $\int dt\, IV$ (Figure 2) with gun voltage $V = I[R_S + L(dI/dt)]$. This I_o is somewhat below the theoretical value of 208 KA with bias flux ψ = 26

mW, or the measured value of 220 KA as I_o is defined in the SSPX database. The gun voltage (Figure 3), which follows from these choices and Eq. (1), is also in reasonable agreement with the measurements.

The remaining parameter f_K is discussed in Section 3.

3. Results

Our simulation of the temperature and magnetic field for Shot 4624 is shown in Figure 4. The core temperature (r = 0) is plotted, labeled TO in the figures. For simplicity we ignore impurities and we consider only the electron channel, not coupled to ions, and we hold the density constant at $n = 10^{20}$.

The magnetic field in Figure 1 is to be interpreted as the poloidal field at the wall at the midplane, corresponding to a field energy $E = 2B^2R^3$ MJ with flux conserver radius R. The parameter $f_K = 0.4$, held constant throughout the shot. This value, adjusted to obtain agreement with the measured peak field in the Formation phase, also gives reasonable agreement with the field throughout the shot. This value of f_K is similar to that fitting most shots, possibly representing a "short-circuit" of injected helicity inside the gun that never reaches the main flux conserver volume. The actual value may be larger when sheath voltage is accounted for (Section 6). Upcoming experiments will attempt to improve f_K using new bias coils now being installed in SSPX.

The peak temperature is 0.12 KeV, in good agreement with the Thomson scattering measurement, is obtained using the same parameters in the Rechester-Rosenbluth thermal diffusivity that fit CTX [2], as currently written into the SPHERE code. The temperature is measured at the peak of the sustaining current ($t \approx 1$ ms), while in the simulation the peak temperature occurs at $t \approx 2$ ms during the weakly sustained period when the field is slowly decaying and the turbulence enhancement factor g_P appearing in the Rechester-Rosenbluth formula is order unity. Lower temperatures earlier in the shot reflect larger values of g_P as shown in Figure 5, which plots the $g_P(r)$ profile at four successive times during the shot.

That the Sustainment Bank still plays an important role when the peak temperature occurs is verified by comparing Figure 4 with sustainment to Figure 6 with no sustainment (Formation Bank only). Without sustainment, the field decays more rapidly and the peak temperature is somewhat less. The actual temperature during formation would depend on whether or not impurities are negligible as assumed, and the actual density during the formation phase.

The effect of classical heat losses is shown in Figure 7, for which the Rechester-Rosenbluth transport term is turned off, giving a 50% increase in temperature. For this

purpose the ion and electron temperatures are assumed to be equal, in which case ion collisional heat conduction is dominant. We do not include a neoclassical correction, which is difficult to estimate for the spheromak and should be less important than in tokamaks because in a spheromak the toroidal and poloidal fields are about equal.

Finally, parallel heat conduction is added with $\chi_{PARALLEL} = v_e^2/\nu_e$ depending only on quantities already in the SPHERE code. In order to continue to utilize the radial heat transport equation in SPHERE, we approximate parallel heat conduction as radial heat conduction through the rough correspondence $dL = 2\pi N dr$ giving a total line length $2\pi Na$ with $N = (2\pi aB/\mu_o I_o)$, previously shown to explain line lengths in NIMROD simulations (Appendix A). Then the effective radial thermal diffusivity is:

$$\chi_{EFFECTIVE} = \chi_{PARALLEL}/(2\pi N)^2 \qquad (4)$$

The effect of including this $\chi_{EFFECTIVE}$ is shown in Figure 8, giving a maximum temperature of T = 0.03 Kev, four times less than the measured value.

4. Extrapolation to Long Pulses and Improved Efficiency

Using Eq. (1), the magnetic buildup equation in SPHERE is given by:

$$dE/dt = f I^2 R_S - E/\tau \qquad (5)$$

where τ is the decay time and f is the overall gun efficiency, Eq. (3). Convenient units are megajoules, megamperes, milliseconds and milliohms, giving $B/I \approx I_{toroidal}/I$ in SSPX. For large τ so that dissipation can be ignored, integrating Eq. (5) gives approximately the following formula for the current amplification:

$$B/I \approx (2R^3)^{-1/2} (t\, f\, R_S)^{1/2} \qquad (6)$$

where t is the pulse duration.

For typical parameters of experiments to date, this gives $B/I \approx 1$. This numerical fact, rather than any limit in principle, is sufficient to explain the apparent limitations on

current amplification in these experiments. For example, for SSPX, R = 0.5, typically $f \approx 1/6$, and in the above units $(t\,R_S) = 0.2 \times 4 = 0.8$ for the Formation Bank and $(t\,R_S) = 1 \times 2 = 2$ for the Sustainment Bank, giving B/I = 0.7 - 1.2; and similarly for CTX, except that $f \approx 1/2$, accounting for a sometimes higher amplification in CTX (a factor $\sqrt{3}$ by our formula). Efforts to increase B/I in SSPX have been frustrated by the dependence of all three factors t, f and R_S on $\lambda_{GUN}/\lambda_o \equiv I_o/I$ (e.g. $f \propto \lambda_o/\lambda_{GUN} = I_o/I$, $R_S \propto (1 - I_o/I)$, and $t \propto (1 - I_o/I)^{1/2}$, giving a broad optimum at $I_o/I \approx 0.5$).

If we assume that R_S is given by Nature, then, aside from optimizing f, the only way to increase current amplification by Eq. (6) is by lengthening t using the pulse line capability of the SSPX Sustainment Bank. The ultimate limit on useful pulse length is τ, the dissipation time. This is where heat transport along open field lines matters. Parallel transport along open field lines could ultimately be the limit on temperature. But as long as radial transport determines the temperature, the beta obtained by ohmic heating is relatively fixed both for classical and turbulent transport (Appendix B), giving $T \propto B^2/n$. Then, unless n runs away, T climbs with B so as to maintain $t < \tau$ and buildup continues more or less forever.

To see the benefits of longer pulses, we extend Shot 4624 sustainment, simulated in Figure 4, by holding the gun current I constant after it reaches its peak value ($\approx$ 200 KA at $t \approx 0.001$ s in Figure 4). We then shut off the current at t = 0.003 s and watch the decay.

Results are given in Figure 9. Despite appearances in Figure 4 (Shot 4624), where the low current in this shot is barely able to hold up the field, the extended pulse injects an additional 100 KJ of gun energy, giving a maximum B = 0.36 T (nearly double) and a maximum temperature T = 0.22 KeV (also nearly double). Characteristically, the maximum temperature occurs after turnoff when turbulence enhancement of transport diminishes as discussed in Section 5.

To see the benefit of improved efficiency, in Figure 10 we repeat the calculation of Figure 4 with $f_K = 1$ giving the ideal efficiency, $f = I_0/I$. The improved efficiency increases the field and temperature for this short-pulse case about as much as did the longer pulse at poorer efficiency, in Figure 9. The improvement would be less if, as noted earlier, f_K in Shot 4624 is higher taking sheath voltage into account (Section 6).

Simultaneously improving the efficiency and extending the pulse would give still higher fields and temperatures. Higher charging voltage yielding higher gun current, well

within SSPX capability, would yield even higher fields and temperatures, if the empirically-derived spheromak impedance is maintained as assumed in the model.

5. Toward a Standard Model for Spheromaks

Our success in predicting temperatures in SSPX suggests that SPHERE physics could serve as a "standard model" for spheromaks that focuses theoretical attention on critical uncertainties expressed in terms of a few fitting parameters connecting theory and experiment. As we have seen, one of these parameters -- the Rechester-Rosenbluth χ in SPHERE -- appears to yield correct temperatures if the magnetic field is calculated correctly. The greater challenge, and the greatest uncertainly in using SPHERE to extrapolate to future experiments, is the spheromak resistance parameter κ appearing in Eq. (1), discussed in Section 6.

In this section we will review the χ calculation in SPHERE, as an example use of the standard model. The main idea of the standard model, the one that makes it possible to calculate χ and temperatures, is the paradigm of a flux core spheromak always evolving self-similarly around a preferred state of magnetic stability.

The rationale for the model has two parts. The first, based both on measurements and on theoretical expectations, reflects the fact that, whatever the actual magnetic structure, most of the magnetic energy is contained in symmetric n = 0 components that have the form of an open-line flux core at the geometric axis which is tied to the bias flux ψ, surrounded by a spheromak with closed magnetic surfaces and an energy close to that of the lowest Taylor state with eigenvalue λ_o -- as in J. B. Taylor's papers, in Corsica equilibria, and in NIMROD calculations [4]. In the model, to maintain force balance the flux core radius shrinks as the spheromak field grows during buildup, as shown in Appendix B. This model allows us to keep books on magnetic energy and helicity in a simple way, through the relation $E = (\lambda_o/2\mu_o)K$ used to calculate the "fundamental efficiency" in Section 2. It also allowed us to calculate the length of field lines at steady state in NIMROD given in Appendix A and cited in Section 3.

The second part of the rationale -- more controversial and more theoretically based -- is the expectation that spheromak dynamics is dominated by instabilities that continuously force the magnetic state to a preferred state of stability, sometimes described

by a fixed λ profile (motivated by $\nabla\lambda$ as the drive for tearing) though this is not the essential point (for example, instead of tearing the preferred state may be determined by pressure driven modes, or non-linear helicity transport).

To calculate χ using the standard model, we start from Faraday's law, multiplied by B to obtain a magnetic energy propagation equation with Poynting vector P(r). (Alternatively, we could consider helicity transport, but the result would be the same, since $<\lambda> \approx \lambda_o$ for the standard model.) Integrating the magnetic propagation equation gives [2]:

$$(2\pi)^2 ar\,|P(r)| \quad = \quad |\,-\,h(r)[P\,-\,P_\Omega(a)]\;-\,P_\Omega(r)\,| \;\equiv\; g_p(r)P_\Omega(r) \qquad (7)$$

Here P, from Eq. (2), is the portion of the gun power feeding dE/dt, coming from the boundary condition on P(r) at r = a. $P_\Omega(r)$ is the integral of ηj^2 from 0 to r (cylinder model) and $h(r) = \int^r B^2 rdr / \int^a B^2 rdr$ is the field form factor defined in Ref. [2]. The standard model has entered in assuming that h(r) is constant in carrying out the integration. Otherwise, Eq. (7) is exact. All quantities other than h(r) can be time dependent, representing buildup, steady state or decay.

To maintain the preferred state h(r) constant in time, it is generally necessary for magnetic energy to flow from the edge to the core during injection from the edge, and from the core to the edge during decay to maintain the low-temperature edge against greater dissipation there. This is captured in P(r), which we interpret as being proportional to the turbulence required to maintain B near the preferred state, having the form $P(r) = v^*<\delta B^2>/2\mu_o$ with fluctuations $<\delta B^2>$, time-averaged if turbulence occurs in bursts. In SPHERE we use P(r) to calculate the Rechester-Rosenbluth heat transport coefficient $\chi = v_e L_c <\delta B^2>/B^2 \propto L_c\, P(r)/v^*$ [3]. The free parameter is L_c/v^* which for an expected correlation length $L_c = \pi R \approx 6a$ requires $v^* = v_A$ (Alfven speed) based on earlier calibrations to temperature measurements in CTX [2] (in SPHERE, P(r) is defined to be 2 times our definition here, giving $L_c = 3a$). Then energy confinement scales with the local magnetic Reynolds number $S \propto P_\Omega(r)^{-1}$, enhanced by the factor $g_p(r)$ that is fully determined by Eq.(7) together with the standard model assumption that h(r) is a known constant function of r.

The interesting physics is contained in the turbulence enhancement factor $g_p(r)$. For the non-physical case λ and η constant in r, during decay (P = 0), $g_p = 0$ everywhere, automatically; the field decays exactly self-similarly with no turbulence and there is no heat transport due to magnetic turbulence. Even in realistic cases, though g_p increases when power is applied, it hovers near or below unity in quasi steady-state, as we found for SSPX Shot 4624 in Figure 5. The scaling of temperature with g_p is given in Appendix C for a zero-D approximation to SPHERE.

A serious theoretical challenge to the standard model comes from NIMROD [4], though the results of Figure 8 make it difficult to explain SSPX based on NIMROD simulations. In NIMROD, during gun injection all field lines carrying current remain open, attached to the gun. This in itself would not contradict the standard model if the open lines were very long and chaotic in the manner assumed by Rechester and Rosenbluth -- apparently not the case in NIMROD. In the Rechester-Rosenbluth picture, any pair of field lines initially separated in radius occasionally almost touch (with correlation length $\approx \pi R$ [3]) as the lines wind their way to the wall by random walk between magnetic islands. In that case, Rechester and Rosenbluth find that the derailing of parallel heat flow by radial diffusion at the touch points gives larger heat transport to the wall than would parallel heat conduction all the way to the wall -- the reason being that they find χ (radial) $\propto \delta B^2$ and the line length $L \propto \delta B^{-2}$, giving $\chi(\text{radial})/a^2 > \chi(\text{parallel})/L^2$ unless magnetic fluctuations are very large [3].

6. A Model for the Spheromak Resistance R_S

The input power to the spheromak, P in Eq. (2), depends on the spheromak resistance R_S, which must be determined independently. Here we present a model for R_S in sustainment based on an interpretation of the Poynting vector discussed in Section 5. This model relates the spheromak resistance to inductance in the flux core, which can be obtained from gun current and voltage data.

We start by taking r = a in Eq. (7), in order to examine power flow out of the flux core. Using h(a) = 1, we obtain:

$$P = Av^*\langle\delta B^2\rangle/2\mu_o = A_{FC}v^*f\langle\delta B^2\rangle_{FC}/2\mu_o \quad . \qquad (8)$$

The second step equates power flowing into the spheromak with surface area A to power

flowing out of the flux core with surface area $A_{FC} = 2\pi R_C R$, radius R_C and length R (the length of the geometric axis). Also, we have added a factor f (efficiency) to approximate the fact that Eqs. (5) and (7) only account for the spheromak mean field energy.

To evaluate P, we suppose that $<\delta B^2>_{FC}$ represents the time average of localized sawtooth oscillations in which transport occurs during an interval δt when islands overlap and reconnection occurs, following a slow buildup of free energy δW in a time $t = (\delta W / I^2 R_S) = f\delta W/P$ using Eq. (2) [10]. Then:

$$P = f\delta W/t \qquad (9)$$

$$V_{FC} <\delta B^2>_{FC} /2\mu_o = \delta W(\delta t/t) \qquad (10)$$

with flux core volume $V_{FC} = \pi R_C^2 R$. We estimate the free energy as:

$$\delta W = 1/2\ L_{FC}(I^2 - I_o^2) = L_{FC} I^2 (1 - I_o/I)[1 - 1/2\ (1 - I_o/I)] \approx L_{FC} I^2 (1 - I_o/I) \qquad (11)$$

with flux core inductance L_{FC}. (Though normally one would expect $\delta W \propto (1 - I_o/I)^2$ due to some constraint such as helicity conservation [6], helicity is not conserved in the flux core alone.)

Combining Eq. (2) with Eqs. (8) - (10) gives:

$$P = f I^2 R_S = (v^*/w) f\delta W(\delta t/t) = f\delta W/t \qquad (12)$$

with $w = V_{FC}/ A_{FC} = 1/2\ R_C$, which we shall interpret as roughly an island width at the time of overlap of islands at the surface of the flux core. Selfconsistency requires $\delta t = w/v^*$, which says that v^* is the reconnection speed. We estimate t from the Rutherford growth rate $dw/dt = \Delta' <\eta>/\mu_o$ giving $t \approx w\mu_o/\Delta' <\eta> = 1/2\ R_C \mu_o/\Delta' <\eta>$ where Δ' is the tearing parameter and $<\eta>$ is the line-averaged resistivity. Introducing this into Eq. (12) and using Eq. (11) gives R_S in Eq. (1) with coefficient κ given by:

$$\kappa = L_{FC}/t = \alpha\beta\, R_{FC} \qquad (13)$$

$$\alpha = (\Delta' R_C) \qquad (14)$$

$$\beta = (2\pi\, L_{FC}/\mu_o R) \qquad (15)$$

$$R_{FC} = (\langle\eta\rangle RB/\psi) \approx (8\lambda_o/I_o)(ZRB)^{2/5} \qquad (16)$$

where R_{FC} is the classical resistance of the flux core with cross-sectional area $\pi R_C^2 = \psi/B$, $\langle\eta\rangle \approx (4 \times 10^{-8})T_o^{-3/2}$, T_o (at the midplane) $= 0.025(ZRB_{FC})^{2/5}$ by ohmic heating in the open-line flux core, with field B_{FC} in the flux core. Then $R_S \propto (L_{FC}/I_o)(1 - I_o/I)$. The SSPX resistance data base is plotted versus this scaling law in Figure 11 for the Formation Bank and in Figure 12 for the Sustainment Bank.

Note that this interpretation of R_S makes clear why empirically the spheromak load appears as a resistance in SPICE simulations, while its origin lies in inductive magnetic energy. From Eq. (13), the spheromak load represents a voltage drop $IR_S \propto L_{FC}(I/t)$ in which the free energy replacement time t replaces the usual inductive timescale from dI/dt. In relating t to resistive tearing through the Rutherford formula, the essentially inductive spheromak resistance becomes an enhancement of the classical resistance R_{GUN}.

For SSPX Shot 4624, $L_{FC} = 0.6$ μH from a fit to experimental data, giving $\beta = 6$, and $R_{GUN} = 0.3$ mΩ for Z = 2, R = 0.5 and $B_{FC} \approx 2.5B_{WALL} = 0.5$ at the geometric axis (giving $T_o = 0.02$KeV in the flux core). Then $\kappa = 2\alpha$ (mΩ), requiring $\alpha = 5$ to obtain our fitting value $\kappa = 10$ mΩ in Section 2.

We might have expected $\alpha \approx 1$ (though a flattened current profile in the flux core might give a higher value at its surface). Note, however, that a lower α, giving a lower κ, implies that a smaller fraction of the gun power contributes to building the field than is implied by our fit in Section 3 -- due to sheath losses rather than inefficient helicity injection ($f = f_K(R_S/R_{GUN})(I_o/I)$).

Indeed, a lower value of α, and also less scatter in the data than in Figures 11 and 12, is obtained when we attempt to refine the resistance formula to include the sheath voltage $\approx \gamma T_o = \gamma 25\ (ZRB)^{2/5}$ (in volts) and the classical resistive drop IR_{GUN}, using Eq.(16) with $\lambda_o = 10$ for SSPX. Including these terms in the voltage along with IR_S and dividing by I gives a total gun resistance:

$$R_{GUN} = [(ZRB)^{2/5}/ I_o][25\gamma(I_o/I) + 80\{1 + 1/2\ \alpha\beta(1 - I_o^2/ I^2)\}] \qquad (17)$$

where in the last term (R_S) we have retained the exact form of δW from Eq. (11). In Figure 13, we fit Eq. (17) (in mΩ) to SSPX data for different values of the gun current (in MA) at a fixed $\psi = 15$ mW ($I_o = 0.12$ MA) with $\beta = 6$ as found above.

For this model, the remaining scatter in experimental values at the stability threshold $I = I_o$ (where the α term is zero) reflects uncertainties in sheath and gun physics, while scatter in the asymptotic limit $I >> I_o$ (where the γ term is small) reflects uncertainties in flux core stability physics (Δ'). Given the scatter, there is latitude in how we choose the fit, especially near $I = I_o$, giving a lower α and κ for a higher sheath voltage (higher γ). To illustrate this point, the fits in Figure 13 have $\alpha \approx 0.8$ both for the curve labeled FB (Formation Bank) and that labeled SB (Sustainment Bank), but a much larger sheath voltage is required for Formation: $\gamma = 22$, giving a sheath of 417 volts (probably too high). In mirror devices, typically $\gamma = 5$ - 10.

While the rough agreement with experiment in Figure 13 is encouraging, there is as yet no direct evidence of saw tooth behavior in the data; the inductance L_{FC} is purely empirical; and the mechanism for reconnection is unknown.

The earliest attempt to understand the spheromak impedance is given in Reference [5], in which Eq. (1) was first proposed, along with a theoretical model for κ based on mass flow in coaxial guns. Figure 10 in Reference [5] plots Eq.(1) for CTX data, giving κ = 20 - 30 mΩ -- similar to our fit in Section 3 if $T_o = 0.01$KeV in CTX versus our inferred value of $T_o = 0.02$KeV in SSPX Shot 4624. Other attempts to explain the resistance have

been based on radial transport of helicity inside the flux conserver, by time-averaged <v X B> due to tearing (which should be included in NIMROD), and hyper-resistivity due to Rechester-Rosenbluth particle transport (probably too weak [6]).

An alternative theoretical approach might be Rechester-Rosenbluth particle flow, which transports helicity with the particles [7]. Particle flow, appearing directly in v x B, gives much stronger transport than does hyper-resistivity, which is a correction to resistance. Conceptually, with $v^* = v_A$ to fit temperature data (Section 5), helicity transport by radial particle flow inside the flux conserver is a continuation of the coaxial flow in the gun discussed in Ref. [5]. In the gun, energy flows only when $I > I_o$ (force imbalance), giving a magnetic energy flow rate $v_A B^2/2\mu_o$. After the flux core geometry is established, flow out of the flux conserver occurs at a similar rate, but only intermittently during island overlap and reconnection, giving Rechester-Rosenbluth transport.

Transport of helicity by Rechester-Rosenbluth particle flow may be the only theoretical mechanism large enough to explain the data during sustainment, if the MHD <v x B> dynamo included in NIMROD does not do the job. This would appear to require that particles flow up hill in order to reach the dense, high pressure core of the spheromak. But inward particle pinches do occur in tokamaks. It might be useful to search for experimental evidence correlating R_{GUN} from fits to data with particle flow (gas feed, rising n, leaking or recycling particles; see Ref. [5]).

7. Conclusions

The simplified physics model of the SPHERE code, originally calibrated to CTX experiments at T = 0.1 KeV and T = 0.4 KeV, now yields the correct maximum temperatures achieved in SSPX sustainment experiments (T = 0.12 KeV). The dominant energy loss process appears to be Rechester-Rosenbluth heat transport in a tangled magnetic field characterized by a random walk of field lines in space, as would be expected for a mean field with closed flux surfaces together with overlapping islands. NIMROD simulations do not appear to yield this structure, suggesting that reconnection is not treated adequately.

The ability to predict temperatures in SPHERE is based on an assumption that we propose as the “standard model” for spheromaks. Namely, during sustainment a gun-injected spheromak is well approximated by a flux core attached to the gun, surrounded by a spheromak in which time-averaged turbulence levels are self-regulated to maintain an approximate Taylor state. This assumption is sufficient to pin down turbulence levels and associated transport inside the spheromak, as discussed in Section 5.

The main uncertainty in the model is the spheromak resistance in sustainment, needed to calculate the buildup of the field. A tentative model relating the resistance to flux core inductance is given in Section 6, but much work remains to be done. A reliable formula for the spheromak resistance in sustainment is the key to making SPHERE a reliable tool for predicting performance of future experiments and reactors (Section 4). The model in Section 6 is perhaps a starting point.

Finally, the simplified cylinder geometry in the SPHERE model must be improved. Implementing the SPHERE model in the 2-D Corsica transport code is straightforward [8].

References

[1] D. D. Hua, T. K. Fowler and E. C. Morse, "SPHERE -- A SPHeromak Experiment and Reactor Simulation Code," Department of Nuclear Engineering, University of California, Berkeley, UC-BFE-054, March 1, 2000.

[2] T. K. Fowler and D. D. Hua, Journal of Fusion Energy **14**, 181 (1995)

[3] A. B. Rechester and M. N. Rosenbluth, Phys., Rev. Lett. **40**, 38 (1978).

[4] C. R. Sovinec, J. M. Finn and D. del-Castillo-Negrete, "Formation and Sustainment of Spheromaks in the Resistive MHD Model," LA - UR - 00 - 03229, July, 2000 (to be published).

[5] C. W. Barnes, T. R. Jarboe, G. J. Marklin, S. O. Knox and I. Henins, Phys. Fluids B **2**, 1871 (1990).

[6] T. K. Fowler, "SSPX Simulation Model," UCRL - ID - 135797, September 30, 1999.

[7] T. K. Fowler, "Particle Driven Helicity Transport," July 24, 2000.

[8] D. D. Hua, E. B. Hooper and T. K. Fowler, "Modeling Electron Heat Transport During Magnetic Field Buildup in SSPX," UCRL - ID - 128656, October 1997.

[9] T. K. Fowler, "Consequences of Open Field Lines During Gun Injection into Spheromaks," 2nd Revision, November 2, 2000.

[10] N. Mattor, Phys. Plasmas **3**, 1578 (1996).

Appendix A. Length of Open Field Lines

We approximate the bias field $B_o = (\mu_o I_o/2\pi a)$ with a = R/2 and multiplication $N = B/B_o$ and the plasma volume $V = 2\pi^2 a^3 = \pi^2 R^3/4$ (cylinder model). Then, for $f_K = 1$ giving $f = I_0/I$ with $I_0 = \lambda_o \psi/\mu_o$ (Section 2), magnetic steady state found by setting the right hand side of Eq. (5) equal to zero gives, after a little algebra:

$$fIV_S = (\lambda_o\psi/\mu_o)V_S = E/\tau = (V/\tau)(B^2/2\mu_o) = (\lambda_o^2 R/8\mu_o\tau)N^2\psi^2 \qquad (A1)$$

$$N = [(8/\lambda_o R)(V_S\tau/\psi)]^{1/2} \approx (2V_S\tau/\psi)^{1/2} \qquad (A2)$$

where $\tau = (\mu_o/2\eta\lambda_o^2)$ is the decay time.

For a fixed η, this result is valid whether or not field lines are open. For open lines, following Reference [8], we interpret N as the winding number -- the number of times fields lines are wound up inside the flux conserver -- giving a length $L^* = 2\pi Na$ as assumed in the calculations for Figure 8, Section 2, where L^* is the mean length of lines carrying maximum current (reciprocal of the average reciprocal length). As is shown in Reference [8], Eq. (A2) correctly predicts the line lengths found in NIMROD calculations (allowing for a different definition $\tau = (\mu_o R^2/\eta)$in Ref. [4]).

The parameter N can also be interpreted as a winding number even if lines are closed, by analogy with a coil omitting the connections from winding to winding. Closed or open, $B \approx N(\mu_o I_o/2\pi a)$ as if only a fraction I_o of the gun current I is diverted into the spheromak, where it is wound up N times, subsequently reconnected (closed) or not (open). However, unlike the open-line case in which the spheromak current density saturates at $j = V/\eta L^*$ (voltage V) [4], if reconnection causes radial transport to dominate inside the spheromak, then τ increases with B so that no steady state occurs, as discussed in Section 5. The open-line flux core current I does saturate, but buildup of the spheromak current continues if $I > I_o$. The gun current I saturates not far above I_o, due to instability, depending on the magnitude of κ in Eq. (1).

Appendix B. Force Balance in the Standard Model

By the assumptions of the standard model, the field changes self-similarly so that calculating the force balance along the interface between the flux core (FC) and the spheromak (SP) can be reduced to the force balance at any chosen location. Then we can write the force balance equation as:

$$B_{FC} \approx \psi/\pi R_C^2 = B_{SP} \equiv \alpha(E_{SP}/V_{SP})^{1/2} \qquad (B1)$$

where R_C is the flux core radius at a chosen location on the flux core - spheromak interface (e.g. the midplane), ψ is the bias flux (constant) and E_{SP} and V_{SP} are the magnetic energy and volume of the spheromak, and we take α as approximately constant. Differentiating by time and dividing each side by B_{FC} (= B_{SP}) gives:

$$- 2R_{FC}^{-1}dR_{FC}/dt \quad = \quad 1/2\ [E_{SP}^{-1}dE_{SP}/dt \ + V_{SP}^{-1}dV_{FC}/dt] \qquad (B2)$$

where on the right we take $dV_{SP}/dt = - dV_{FC}/dt$ to conserve total volume. Introducing $V_{FC} = L\pi R_C^2$, taking its derivative and rearranging terms gives:

$$[1+1/2(V_{FC}/V_{SP})]R_C^{-1}dR_C/dt \approx -1/4\ [(E_{SP}^{-1}dE_{SP}/dt) + (V_{FC}/V_{SP})(L^{-1}dL/dt)] \quad (B3)$$

Eq. (B3) says that R_C shrinks as long as E_{SP} grows -- the more so if also $dL/dt > 0$ (a small effect by the time that $V_{FC}/V_{SP} << 1$). Then at constant ψ, if R_C shrinks, $B_{FC} \approx \psi/\pi R_C^2$ grows, and B_{SP} grows to maintain force balance, and current amplification grows. Compression and current amplification only stagnate if dE_{SP}/dt stagnates.

The actual dynamics of helicity propagation would not alter the conclusions. If there is a preferred λ profile (assumption (ii)), the dynamics only delays the relaxation to this profile and changes nothing in the long run. Moreover, it can be shown that E_{SP} is rather insensitive to details of the λ profile. Also, note that we allow L to grow, as in a lengthening "doughhook." An asymmetric doughhook flux core can also be described by energy flow out of the doughhook into a surrounding spheromak -- with no real change in Eq. (B3) and its consequences. Otherwise, as long as the energy in asymmetries is small, focusing on the symmetric mean field is a useful concept whatever the actual structure.

Appendix C. Zero-D Heat Transport Model

We approximate the heat diffusion coefficients in the SPHERE code [1], evaluated in the core (r = 0), as follows (T in KeV, n in units of 10^{20}, otherwise MKS units):

$$\chi_{MAG} = 3av_e(g_P/S) = 1.14(g_P/T^{3/2})(nT/B^2)^{1/2} = 5.7\ g_P(\beta^{1/2}/T^{3/2}) \qquad (C1)$$

$$\chi_{CLASS} = (\nu r_L^2)_{ION} = 0.36\ T^{-3/2}(nT/B^2) = 9\ \beta\ T^{-3/2} \qquad (C2)$$

$$\chi_{GYROB.} = 0.6(T^{-3/2}/aB^2) \quad \text{(Ref. [5])} \quad = 15\beta\, T^{-3/2}(T^2/na) \quad \text{(C3)}$$

where we assume equal ion and electron temperatures and we have used $S = av_A\, \mu_o/\eta$, $\eta = 4 \times 10^{-8}\, T^{-3/2}$ and $\beta = 0.04(nT/B^2)$.

We introduce these coefficients into the energy balance for ohmic heating of electrons in the core:

$$\eta j^2 = 3/2\ nT(\chi_{MAG} + \chi_{CLASS} + \chi_{GYROB.})/a^2 \quad \text{(C4)}$$

with $j = \lambda_o B/\mu_o = 2.5\ B/a\mu_o$. The result can be written as:

$$1 = 1.6\ g_P\,(\beta/\beta_C)^{3/2} + (\beta/\beta_C)^2\,(1 + 1.6(T^2/na)) \quad \text{(C5)}$$

where $\beta_C = 0.17$ is the solution for classical transport only.

The gyroBohm term is irrelevant until $T = 0.8(na)^{1/2} = 0.4\sqrt{n}$ in SSPX.

Solutions of Eq. (C5) neglecting $\chi_{GYROB.}$ are given in Table 1 for ascending values of the turbulence enhancement factor g_P.

Table 1. Zero-D Calculations of Peak Electron β versus g_P in the Core

g_P	β/β_C	β	
0	1	0.17	
0.5	0.76	0.13	
1.0	0.57	0.10	SSPX Sustainment
5.0	0.24	0.04	CTX Decay
10.0	0.16	0.027	

Fig. 1

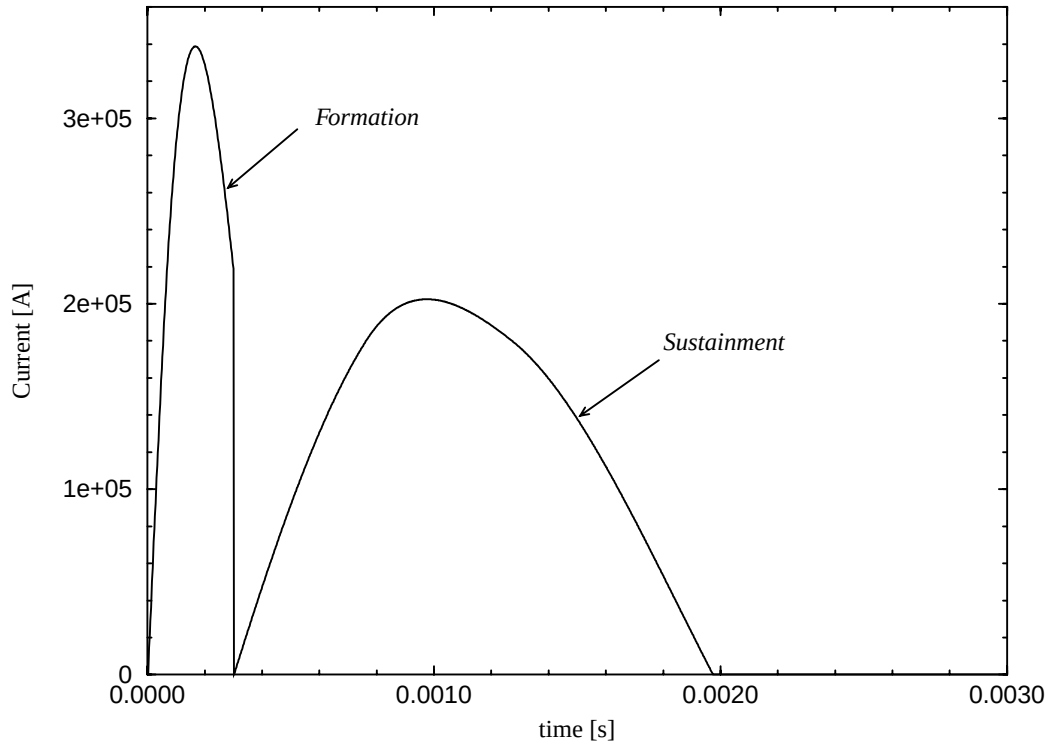
Formation
Sustainment
Current [A]
3e+05
2e+05
1e+05
0
0.0000
0.0010
0.0020
0.0030
time [s]

Fig. 2

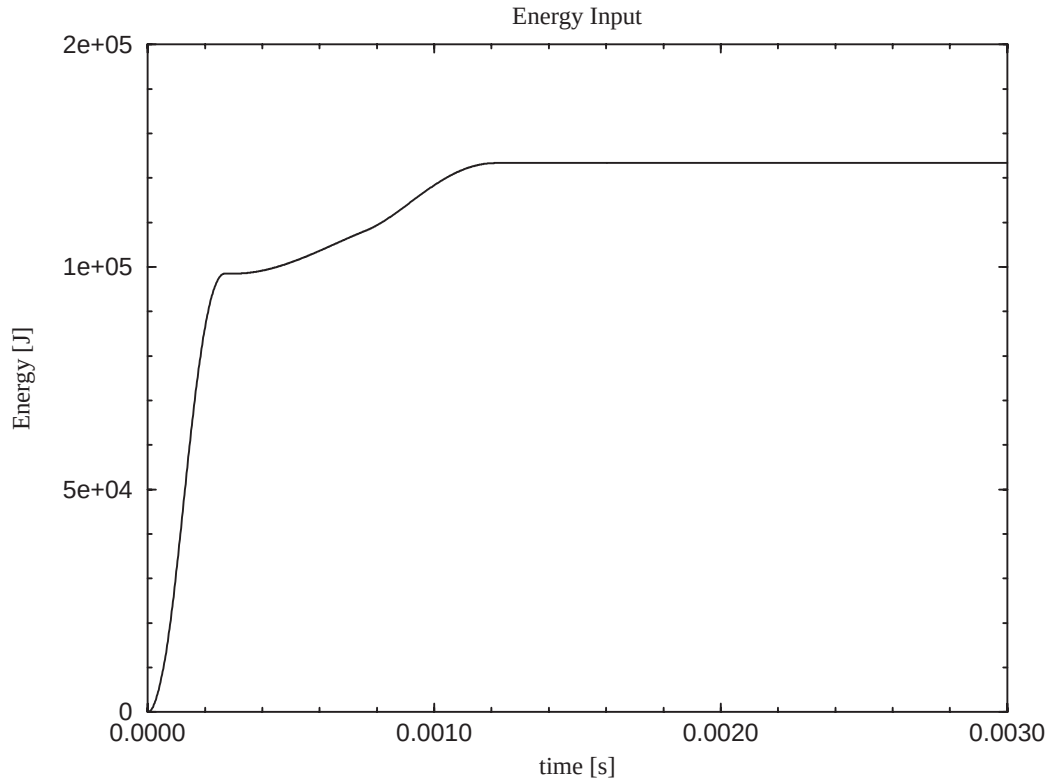
Energy Input
Energy [J]
2e+05
1e+05
5e+04
0
0.0000
0.0010
0.0020
0.0030
time [s]

Fig. 3

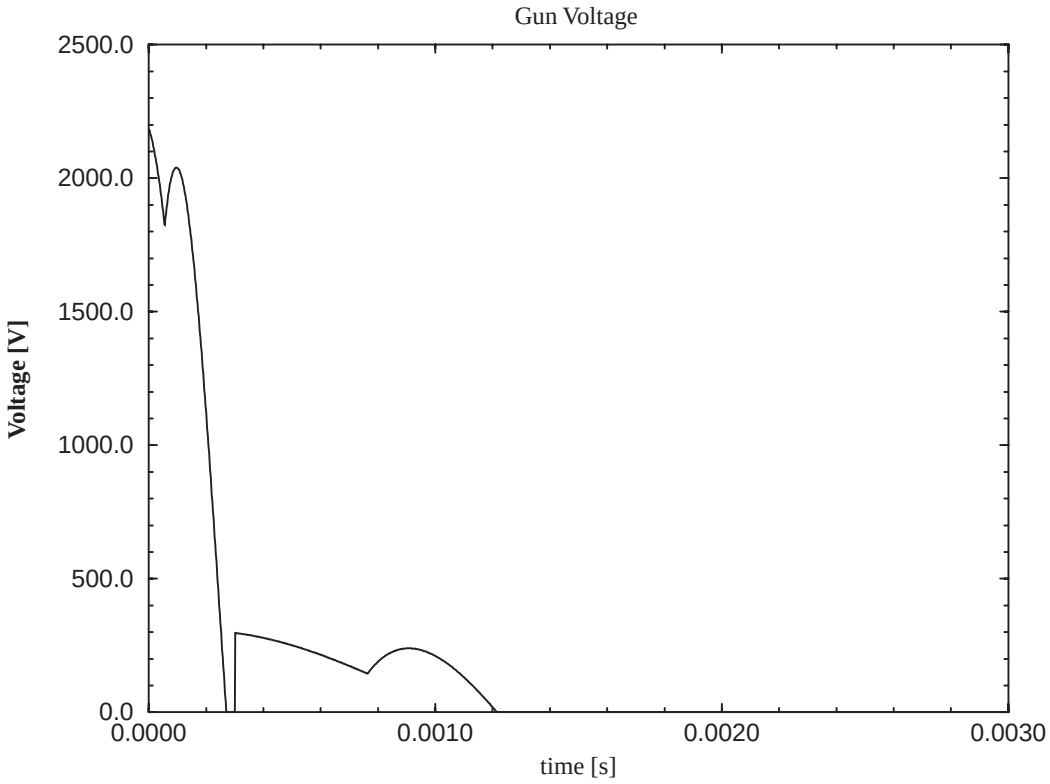
Gun Voltage
2500.0
2000.0
1500.0
1000.0
500.0
0.0
Voltage [V]
0.0000
0.0010
0.0020
0.0030
time [s]

Fig. 4

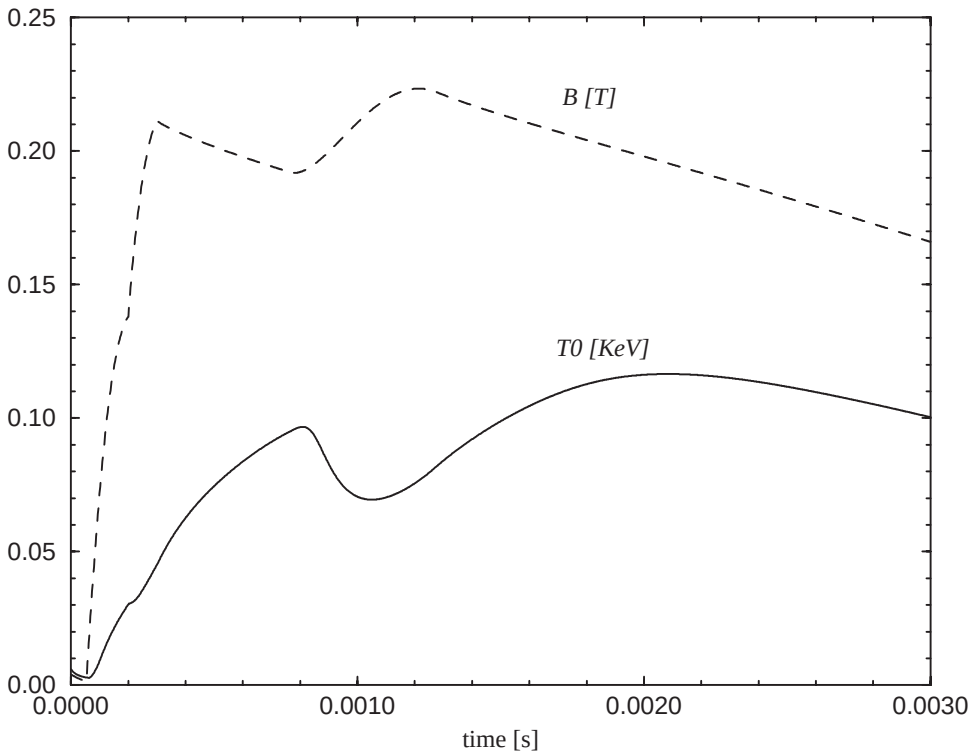
0.25
0.20
0.15
0.10
0.05
0.00
B [T]
T0 [KeV]
0.0000
0.0010
0.0020
0.0030
time [s]

Fig. 5

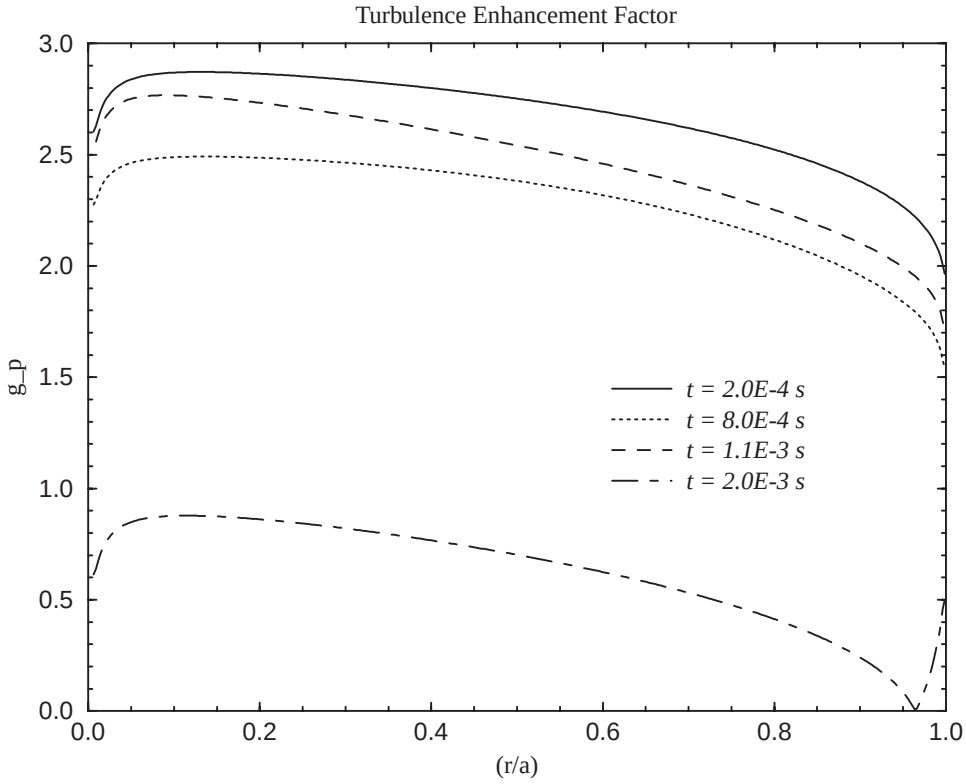
Turbulence Enhancement Factor
3.0
2.5
2.0
1.5
1.0
0.5
0.0
g_p
0.0
0.2
0.4
0.6
0.8
1.0
(r/a)
t = 2.0E-4 s
t = 8.0E-4 s
t = 1.1E-3 s
t = 2.0E-3 s

Fig. 6

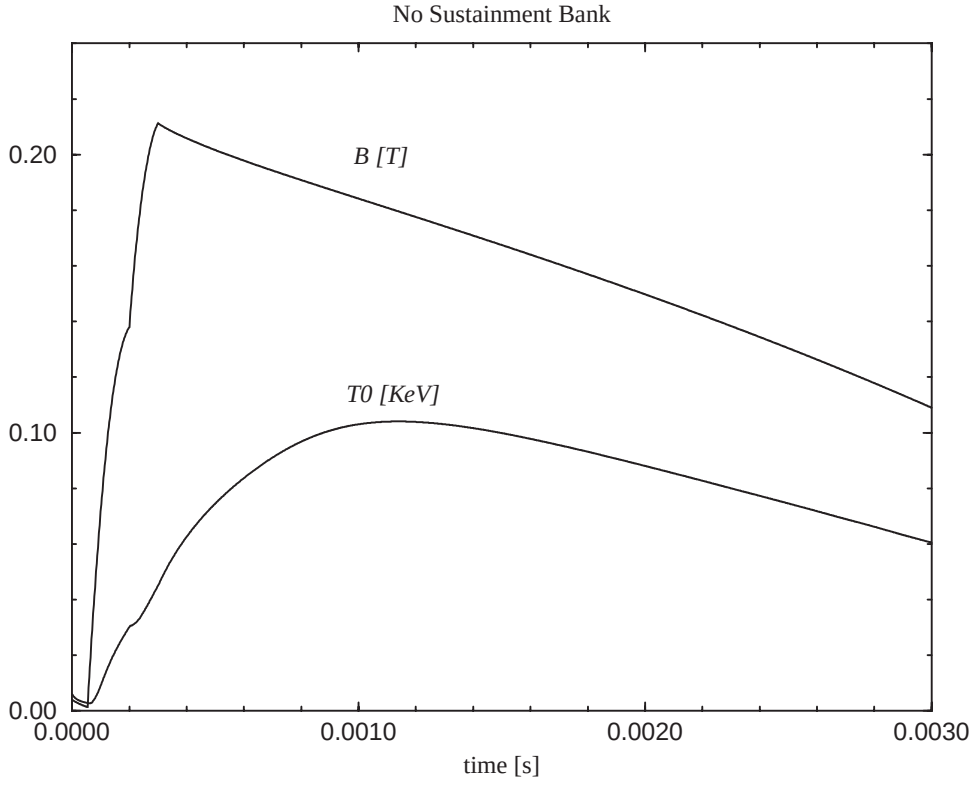
No Sustainment Bank
0.20
0.10
0.00
0.0000
0.0010
0.0020
0.0030
time [s]
B [T]
T0 [KeV]

Fig. 7

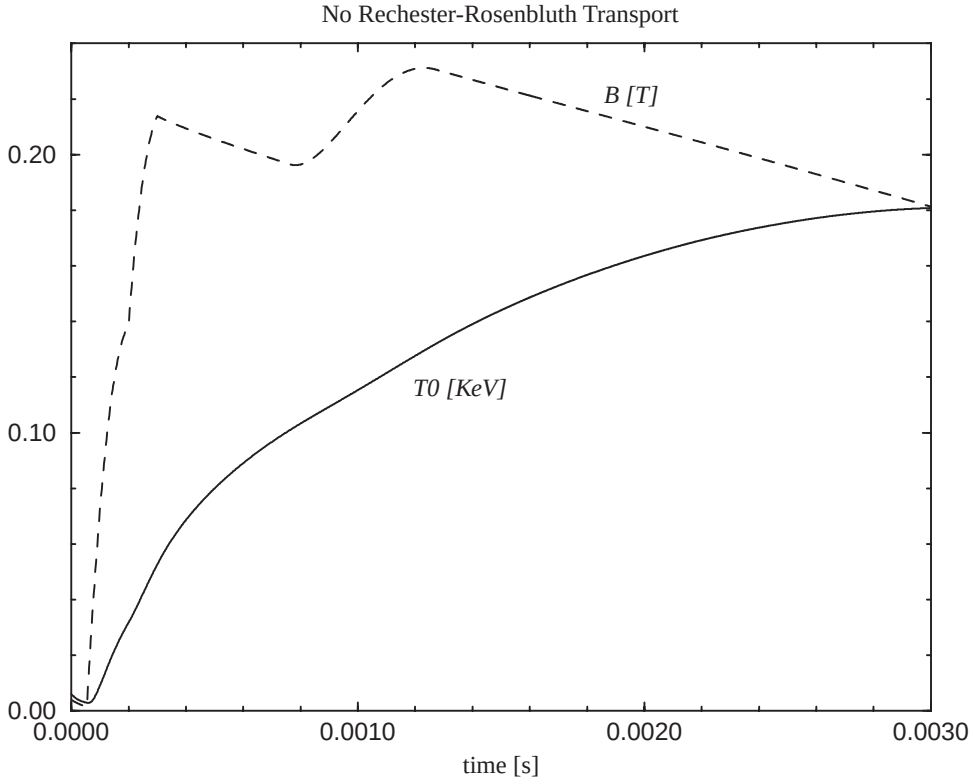
No Rechester-Rosenbluth Transport
B [T]
T0 [KeV]
0.20
0.10
0.00
0.0000
0.0010
0.0020
0.0030
time [s]

Fig. 8

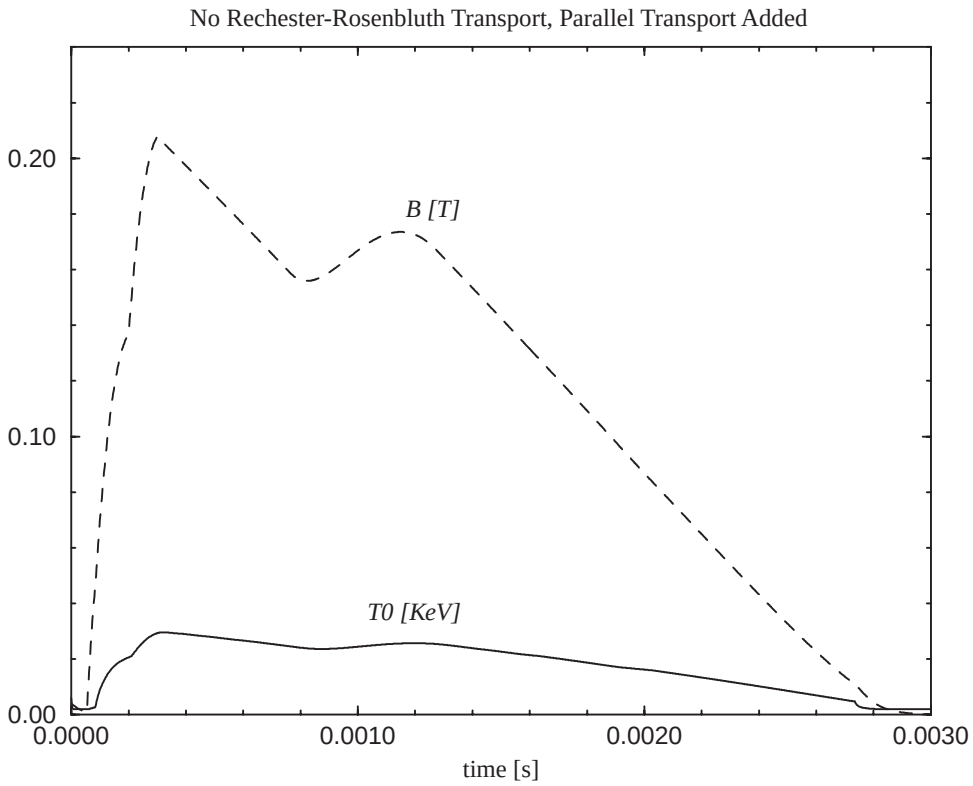
No Rechester-Rosenbluth Transport, Parallel Transport Added
B [T]
T0 [KeV]
0.20
0.10
0.00
0.0000
0.0010
0.0020
0.0030
time [s]

Fig. 9

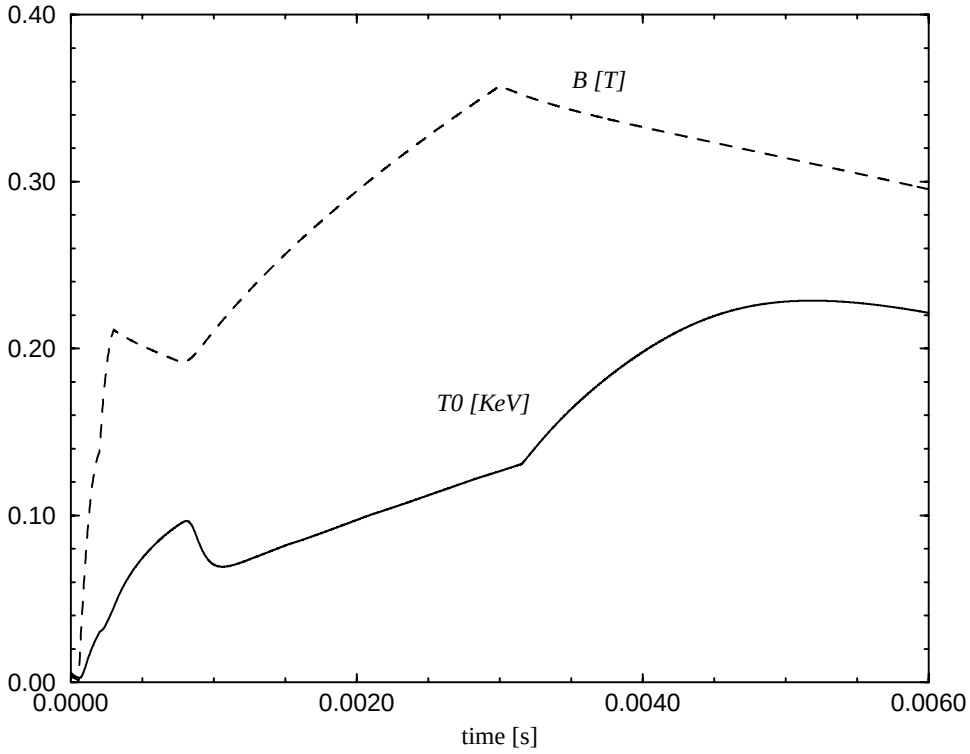
0.40
0.30
0.20
0.10
0.00
0.0000
0.0020
0.0040
0.0060
B [T]
T0 [KeV]
time [s]

Fig. 10

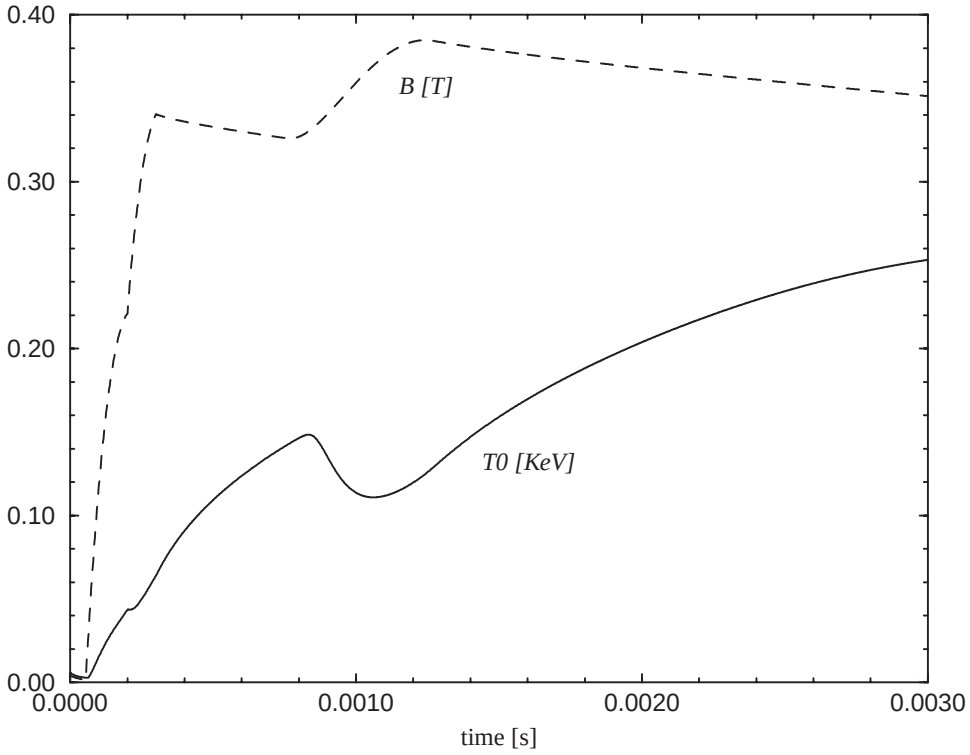
0.40
0.30
0.20
0.10
0.00
0.0000
0.0010
0.0020
0.0030
B [T]
T0 [KeV]
time [s]

Fig. 11

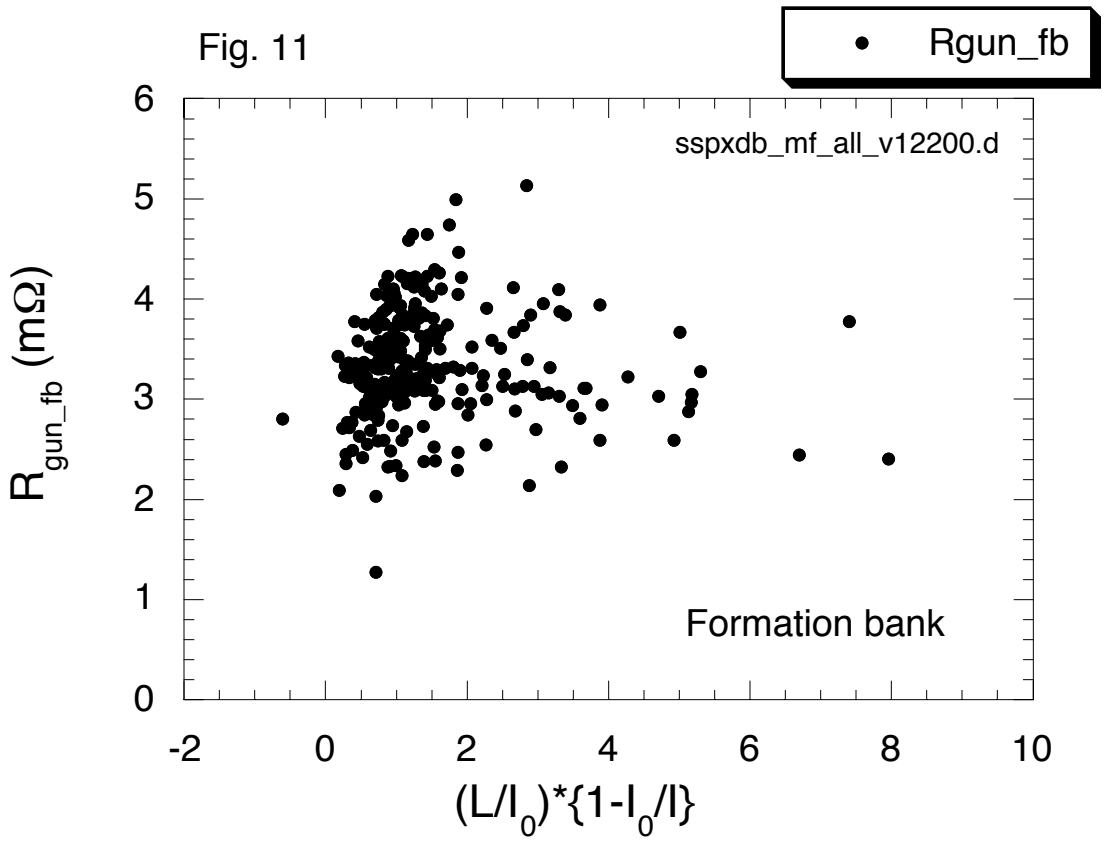
Rgun_fb
sspxdb_mf_all_v12200.d
Formation bank
R_{gun_fb} (mΩ)
$(L/I_0)*\{1-I_0/I\}$
0
1
2
3
4
5
6
-2
0
2
4
6
8
10

Fig. 12

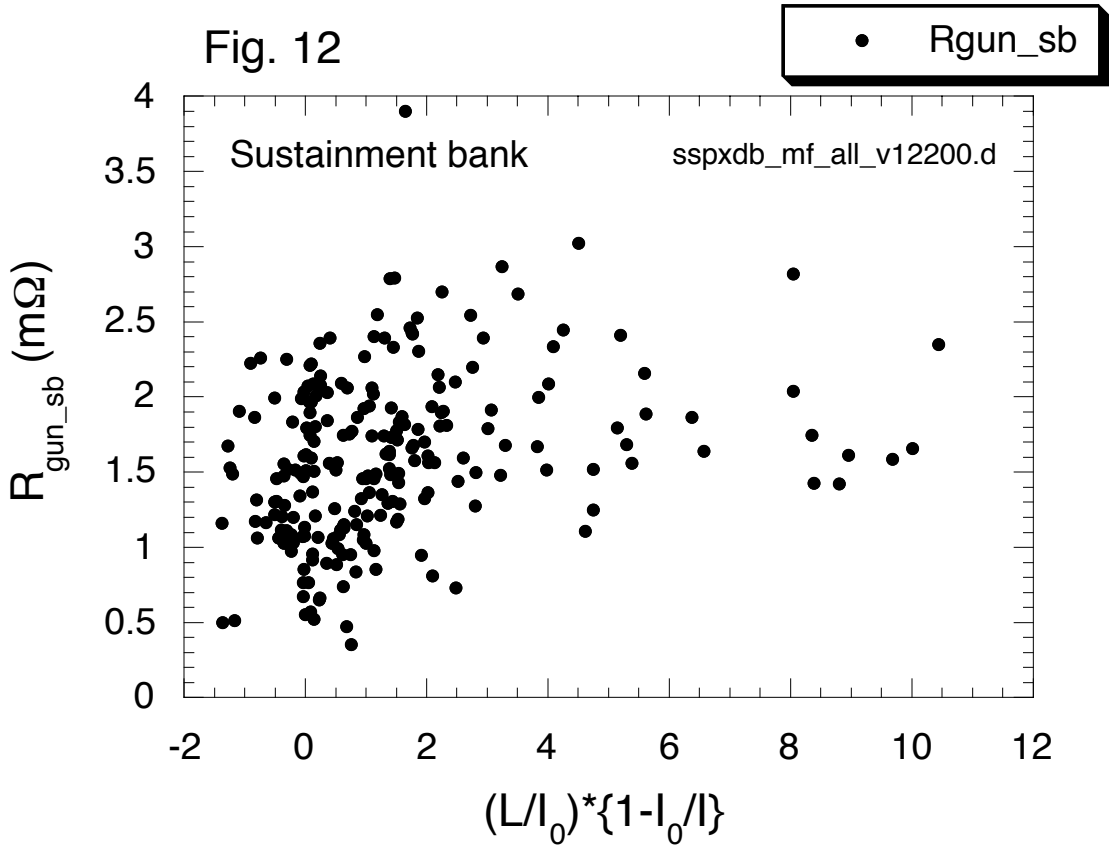
Rgun_sb
Sustainment bank
sspxdb_mf_all_v12200.d
R_{gun_sb} (mΩ)
$(L/I_0)*\{1-I_0/I\}$
0
0.5
1
1.5
2
2.5
3
3.5
4
-2
0
2
4
6
8
10
12

Fig. 13

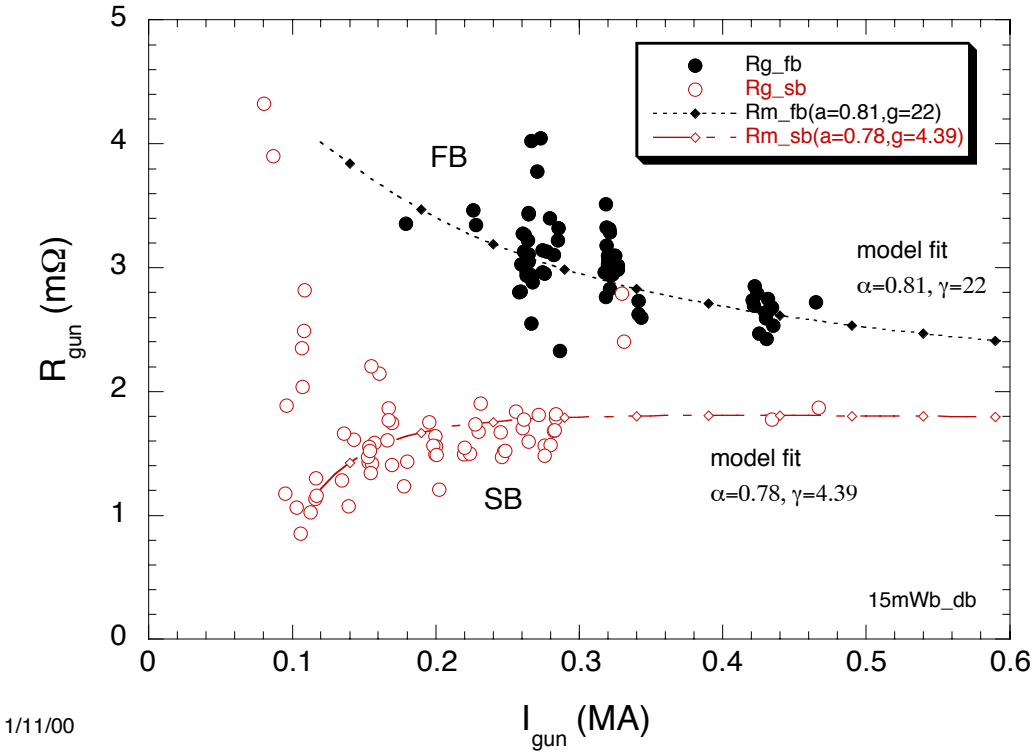
Rg_fb
Rg_sb
Rm_fb(a=0.81,g=22)
Rm_sb(a=0.78,g=4.39)
FB
SB
model fit
α=0.81, γ=22
model fit
α=0.78, γ=4.39
15mWb_db
R gun (mΩ)
I gun (MA)
0
1
2
3
4
5
0
0.1
0.2
0.3
0.4
0.5
0.6

1/11/00